1521-0103/378/1/31–41$35.00
THE JOURNAL OF PHARMACOLOGY AND EXPERIMENTAL THERAPEUTICS

https://doi.org/10.1124/jpet.120.000486
J Pharmacol Exp Ther 378:31–41, July 2021

The Journal of PHARMACOLOGY And Experimental Therapeutics

A p97/Valosin-Containing Protein Inhibitor Drug CB-5083 Has a Potent but Reversible Off-Target Effect on Phosphodiesterase-6[S]

Henri Leinonen, Cheng Cheng, Marja Pitkänen, Christopher L. Sander, Jianye Zhang, Sama Saeid, Teemu Turunen, Alyaa Shmara, Lan Weiss, Lac Ta, Timothy Ton, Ari Koskelainen, Jesse D. Vargas, Virginia Kimonis, and Krzysztof Palczewski

Gavin Herbert Eye Institute, Department of Ophthalmology (H.L., C.L.S., J.Z., K.P.), Department of Physiology & Biophysics (K.P.), Department of Chemistry (K.P.), and Division of Genetics and Genomic Medicine, Department of Pediatrics (C.C., A.S., L.W., L.T., T.T., V.K.), University of California Irvine, Irvine, California; *Department of Pharmacology, Case Western Reserve University, Cleveland, Ohio (C.L.S.); Department of Neuroscience and Biomedical Engineering, Aalto University, Espoo, Finland (M.P., S.S., T.T., A.K.); and Cleave Therapeutics, Inc., San Francisco, California* (J.D.V.)

Received December 26, 2020; accepted April 29, 2021

ABSTRACT

CB-5083 is an inhibitor of p97/valosin-containing protein (VCP), for which phase I trials for cancer were terminated because of adverse effects on vision, such as photophobia and dyschromatopsia. Lower dose CB-5083 could combat inclusion body myopathy with early-onset Paget disease and frontotemporal dementia or multisystem proteinopathy caused by gain-of-function mutations in VCP. We hypothesized that the visual impairment in the cancer trial was due to CB-5083's inhibition of phosphodiesterase (PDE)-6, which mediates signal transduction in photoreceptors. To test our hypothesis, we used in vivo and ex vivo electroretinography (ERG) in mice and a PDE6 activity assay of bovine rod outer segment (ROS) extracts. Additionally, histology and optical coherence tomography were used to assess CB-5083's long-term ocular toxicity. A single administration of CB-5083 led to robust ERG signal deterioration, specifically in photoresponse kinetics. Similar recordings with known PDE inhibitors sildenafil, tadalafil, vardenafil, and zaprinast showed that only vardenafil had as strong an effect on the ERG signal in vivo as did CB-5083. In the biochemical assay, CB-5083 inhibited PDE6 activity with a potency higher than sildenafil but lower than that of vardenafil. Ex vivo ERG revealed a PDE6 inhibition constant of 80 nM for CB-5083, which is 7-fold smaller than that for sildenafil. Finally, we showed that the inhibitory effect of CB-5083 on visual function is reversible, and its chronic administration does not cause permanent retinal anomalies in aged VCP-disease model mice. Our results warrant reevaluation of CB-5083 as a clinical therapeutic agent. We recommend preclinical ERG recordings as a routine drug safety screen.

SIGNIFICANCE STATEMENT

This report supports the use of a valosin-containing protein (VCP) inhibitor drug, CB-5083, for the treatment of neuromuscular VCP disease despite CB-5083's initial clinical failure for cancer treatment due to side effects on vision. The data show that CB-5083 displays a dose-dependent but reversible inhibitory action on phosphodiesterase-6, an essential enzyme in retinal photoreceptor function, but no long-term consequences on retinal function or structure.

Introduction

Valosin-containing protein (VCP) is a member of the ATPases associated with a variety of cellular activities protein family, and it is a highly abundant protein accounting for ∼1% of total cellular protein content (Song et al., 2003). Many of VCP's physiologic actions are related to the ubiquitin-proteasome degradation pathway. Missense mutations in the gene encoding the VCP are causative for VCP disease that is characterized by a complex set of clinical manifestations, such as musculoskeletal and neurodegenerative conditions associated with limb-girdle inclusion body myopathy, Paget disease of the bone, frontotemporal dementia, and amyotrophic lateral sclerosis (Watts et al., 2004). In vitro assays of VCP mutants have shown moderately enhanced ATPase activity, increased cofactor binding, and reduced mitofusin levels, providing evidence for a gain-of-function mechanism of the disease (Blythe et al., 2017; Zhang et al., 2017). Early-generation VCP inhibitors NMS873 and ML240

No author has an actual or perceived conflict of interest with the contents of this article.

H.L. was supported by research grants from the Knights Templar Eye Foundation, Silmä- ja kudospankkisäätiö (Eye and Tissue Bank Foundation), the Finnish Cultural Foundation, and the Orion Research Foundation. K.P was supported by National Institutes of Health National Eye Institute (NEI) [Grants R01EY009339-27 and R24EY027283-01]. K.P is the Irving H. Leopold Chair of Ophthalmology and CSO of Polgenix Inc. The authors also acknowledge support from a Research to Prevent Blindness unrestricted grant to the Department of Ophthalmology, University of California, Irvine.
https://doi.org/10.1124/jpet.120.000486

[S] This article has supplemental material available at jpet.aspetjournals.org.

ABBREVIATIONS: ERG, electroretinography; IS, photoreceptor inner segment; LED, light-emitting diode; OCT, optical coherence tomography; ONH, optic nerve head; ONL, outer nuclear layer; OS, photoreceptor outer segment; PDE, phosphodiesterase; ROS, rod out segment; SNARF-1, seminaphthorhodafluor-1; VCP, valosin-containing protein; WT, wild type.

were shown to ameliorate mitochondrial dysfunction and cell death in a drosophila model of VCP disease (Zhang et al., 2017). Of these inhibitors, one is allosteric, and one is ATP-competitive, demonstrating that different VCP-inhibition modalities drive a similar beneficial response. This finding suggests that direct inhibition of VCP activity is the basis for the therapeutic effects. Unfortunately, both NMS873 and ML240 lack suitable pharmaceutical properties for clinical development. Instead, a newer-generation VCP inhibitor, CB-5083, is an orally bioavailable compound (Le Moigne et al., 2017) that has previously reached phase 1 clinical trials for cancer (ClinicalTrials.gov identifiers: NCT02223598 and NCT02243917).

Many types of cancer in humans are associated with elevated VCP expression (Tsujimoto et al., 2004; Yamamoto et al., 2005). CB-5083 is a reversible and competitive inhibitor that is highly specific for the D2 ATPase domain of the ATPases associated with a variety of cellular activities ATPase p97/VCP, making CB-5083 ideal for probing the specific therapeutic benefit of normalizing the upregulated VCP activity in patients (Le Moigne et al., 2017). Promising preclinical data in cellular and rodent cancer models prompted the developer of CB-5083, Cleave Biosciences, to launch a phase 1 trial in 84 patients with solid tumors and multiple myeloma. CB-5083 was documented as clinically safe and generally well tolerated. However, CB-5083 was not successful in achieving the desired endpoints in the cancer trial because it was halted because of suspected off-target activity against phosphodiesterase (PDE)-6. The PDE6 inhibition ostensibly led to visual adverse events consisting of photophobia and dyschromatopsia that were mild, episodic, and self-resolving at lower doses, but these symptoms increased in frequency and severity at increasingly higher doses, ultimately ending the dose-escalation study. Similar side effects have been associated with other drugs in the PDE-inhibitor family, such as sildenafil and vardenafil that are primarily indicated for the treatment of erectile dysfunction (Moschos and Nitoda, 2016; Yafi et al., 2018). Indeed, the chemical structure of CB-5083 is closely related to those of sildenafil and vardenafil (https://pubchem.ncbi.nlm.nih.gov/). Notably, drug doses required to normalize aberrant overactivity of VCP mutants could potentially be much lower than the doses required to drive a cytotoxic response in cancer cells. We postulate that CB-5083 could be repurposed for the treatment of VCP disease after careful dose titration. However, its adverse effects on vision must be investigated at a mechanistic level before other major research efforts concerning therapy of VCP disease are warranted.

Previously, adverse effects on vision associated with clinical administration of PDE5 inhibitors were attributed to potential inhibition of PDE6, an enzyme required for phototransduction in retinal photoreceptors. Since CB-5083 in the previous phase 1 cancer trial caused side effects analogous to those of known PDE5 inhibitors, we hypothesized that these visual impairments could be due to off-target deactivation of PDE6. In the current study, we present a comprehensive analysis of the impact of CB-5083 on retinal phototransduction to evaluate the potential of this off-target effect to impede clinical use of the drug in the VCP-disease setting. From the perspective of drug safety, our data indicate that repurposing CB-5083 for the treatment of VCP disease or other applicable conditions is a viable option.

Materials and Methods

Animals, Compounds, and Drug Regimen. We used mice as a primary model organism. In acute repeated-measures experiments, 2–4-month-old C57BL6/J wild-type (WT) mice were used ($n = 3$ per drug). In addition, heterozygous VCP^{R155H} knock-in mice between 12 and 18 months of age were used in a chronic ocular toxicity trial (CB-5083, $n = 4$; vehicle, $n = 5$). In the terminal phase of this trial, 18-month-old C57BL6/J mice ($n = 3$) were used as a WT control. An independent electroretinography (ERG) recording was performed also in nontreated 24-month-old VCP^{R155H} ($n = 5$) and 19-month-old WT ($n = 7$) mice to further investigate whether VCP^{R155H} knock-in mutation causes alterations to retinal function. VCP^{R155H} mice (later referred to as VCP model mice) recapitulate many clinical features of VCP disease, including muscle, bone, brain, and spinal cord pathology and demonstrate progressive muscle weakness most noticeably from the age of 9 months onward (Badadani et al., 2010; Nalbandian et al., 2012; Yin et al., 2012). The VCP^{R155H} mice were generated at InGenious Targeting laboratory, Inc. by the Dr. V. Kimonis laboratory and have been backcrossed to C57BL/6J for at least 10 generations. VCP^{R155H} mice were also available through the Jackson laboratory (Stock 021968). Both male and female mice were used in this study. Mice were kept under 12-hour light/dark cycle with free access to food and water. Experimental protocols adhered to the Guide for Care and Use of Laboratory Animals and were approved by the institutional Animal Studies Committee at the University of California, Irvine (protocol AUP-18-124 and AUP-19-075) or by the Laboratory Animal Center of the University of Helsinki, Finland (protocol KEK20-014).

CB-5083 was obtained from Cleave Biosciences for in vivo studies and from MedChemExpress (Sollentuna, Sweden) for ex vivo ERG experiments. CB-5083 solids were solubilized in an aqueous 0.5% methyl cellulose (Sigma-Aldrich; M0262) solution to a final concentration of 3 mg/ml. Methyl cellulose solution was used as vehicle control in the chronic CB-5083 trial, wherein the mice were treated with daily oral gavage. Twelve-month-old VCP model mice were treated with 15 mg/kg CB-5083 or vehicle for 6 months. In acute CB-5083 trials, WT mice were treated with vehicle, 15 mg/kg CB-5083, or 30 mg/kg CB-5083 by a single gavage administration 45 minutes prior to initiation of ERG recordings. These doses were chosen based on previous studies in which a minimum gavage dose of 30 mg/kg CB-5083 was used for cancer therapy in mice using a 4-days-on/3-days-off regimen (Anderson et al., 2015; Le Moigne et al., 2017).

Sildenafil, tadalafil, vardenafil, and zaprinast were all purchased from Cayman Chemical Company (Ann Arbor, MI). Drug stocks were first dissolved in DMSO at a 10-mg/ml concentration and dosed at 50 μl volume via intraperitoneal injection 45 minutes prior to ERG recording.

In Vivo ERG. Before scotopic ERG recordings, the mice were dark-adapted overnight, and animal handling before recording was performed under dim red light. The ERG was performed using a Diagnosys Celeris rodent ERG device (Diagnosys, Lowell, MA), as described previously (Orban et al., 2018). Briefly, mice were anesthetized with ketamine (100 mg/kg, KetaVed; Bioniche Teoranta, Inverin Co., Galway, Ireland) and xylazine (10 mg/mg, Rompun; Bayer, Shawnee Mission, KS) by intraperitoneal injection, and their pupils were dilated with 1% tropicamide (Tropicamide Ophthalmic Solution USP 1%; Akorn, Lake Forest, IL) and thereafter kept moist with 0.3% hypromellose gel (GenTeal; Alcon, Fort Worth, TX). An additional 3 minutes were allowed in full dark adaptation before recordings. Light stimulation was produced by an in-house scripted stimulation series in Espion software (version 6; Diagnosys). The eyes were stimulated with a green light-emitting diode (LED) (peak 544 nm, bandwidth 160 nm) using a 6-step ascending flash strength series in 1-log-unit increments between 0.0005 and 50 cd·s/m^2. After scotopic ERG, the mouse eyes were

adapted to a rod-suppressing green background light at 20 cd/m^2 for 1 minute, and this background was maintained during the subsequent photopic ERG recordings. Here, stimulation was performed with a UV LED (peak emission 370 nm, bandwidth ~50 nm) at light-strength increments of 0.1, 1.0, and 10.0 cd·s/m^2 and separately with a green LED (peak emission 544 nm, bandwidth ~160 nm) at 0.3, 3.0, and 30.0 cd·s/m^2. As the short-wavelength cone opsin and medium-wavelength cone opsin sensitivities peak at 360 and 508 nm, respectively, in mice (Nikonov et al., 2006), UV and green LEDs stimulated mouse short- and medium-wavelength cone opsins relatively selectively. LED light emission spectra were measured with a Specbos 1211UV spectroradiometer (JETI Technische Instrumente GmbH, Jena, Germany). The ERG signal was acquired at 2 kHz and filtered with a low-frequency cutoff at 0.25 Hz and a high-frequency cutoff at 300 Hz. Espion software automatically detected the ERG a-wave (first negative ERG component) and b-wave (first positive ERG component) implicit times (latencies) and amplitudes; a-wave amplitude was measured from the signal baseline, whereas b-wave amplitude was measured as the difference between the negative trough (a-wave) and the highest positive peak.

Mouse Serum and Tissue Collection for Drug Level Measurements. Three-month-old C57BL/6J mice (n = 10) were used for these experiments. Mice were terminally anesthetized by 3- to 4-fold overdose of ketamine-xylazine cocktail. Once fully unresponsive, the mouse chest was incised open, a small hole was punctured to the heart's right atrium, and ~0.5 ml of blood was quickly collected and transferred on ice. A perfusion needle was quickly inserted into the left ventricle, and vasculature was perfused with ice-cold saline for 3 minutes using a peristaltic pump. After perfusion, the retinas were quickly excised by performing three incisions starting from the optic nerve head and cutting toward the *ora serrata*, which allowed easy and quick separation of the retina from the rest of the eye cup. We also collected a 10–20-mg biopsy of frontal cortex for retina-brain comparative analysis. Blood was centrifuged at 4°C and 13 500 rpm for 20 minutes, and thereafter the supernatant was collected as a serum sample. Tissue and serum samples were stored at −20°C until analysis.

Liquid Chromatography–Mass Spectrometry. Each serum sample (100 μL) was precipitated with 400 μL of precooled methanol and centrifuged at 17,000*g* for 15 minutes at 4°C. The supernatant was carefully transferred to a SpinX centrifuge tube filter with a 0.45-μm cellulose acetate membrane (Costar, Salt Lake City, UT) and centrifuged at 7,000 *g* for 2 minutes. Filtered samples were dried under vacuum, reconstituted in 100 μL 50% methanol/water, and centrifuged at 17,000*g* for 15 minutes at 4°C. The resulting supernatants were ready for liquid chromatography–mass spectrometry analyses. Retina and brain biopsy samples were homogenized in methanol (2 × 800 μL). The resulting mixture was centrifuged at 17,000*g* for 15 minutes at 4°C. The supernatant was dried under vacuum, reconstituted in 100 μl 50% methanol/water, and centrifuged at 17,000*g* for 15 minutes at 4°C. Ten microliters of the supernatant extracted from serum or tissue samples was injected into an Ultimate 3000 HPLC system coupled with LXQ mass spectrometer (ThermoFisher Scientific, Waltham, MA) with an electrospray ionization unit. The separation was performed on a Proshell EC-18 column (2.7 μm, 3.0 × 150 mm, Agilent, Santa Clara, CA) using a mobile phase consisting of 0.1% aqueous formic acid (A) and acetonitrile (B) at a flow rate of 300 μL·min^{-1}, and the mobile phase gradients and time course were as follows: 0–3 minutes, 80% A/20% B and 3–13 minutes, 80%–10% A/20%–90% B. The signals were detected in the selected reaction monitoring mode, with the m/z values of the parent and the daughter ions set at 414.2 and 397.2, respectively. Serum, retina, or brain samples from mice without drug administration were spiked separately with 0, 1, 3, 10, 30, 100, or 300 nmol authentic CB-5083 compound and then extracted and analyzed, as described above, to generate the standard curves representing the relationship between the amounts of CB-5083 and the areas under the corresponding chromatographic peaks for specific tissue samples.

PDE6 Activity Assay in Bovine ROS Extracts. Each cGMP molecule acted upon by PDE6 releases a free proton when converted to GMP. The accumulation of protons in solution through PDE6 activity was monitored with the pH-sensitive fluorophore 5-(and-6)-carboxy seminaphthorhodafluor-1 (SNARF-1) (Invitrogen, Carlsbad, California) using a previously described method (Baker and Palczewski, 2011) with modifications. Minimally buffered solution (20 mM 3-(*N*-morpholino)propanesulfonic acid, pH 8.0; 150 mM KCl; 10 mM $MgCl_2$; and 1 mM dithiothreitol) was used to dissolve the concentrated stock of PDE6-containing hypotonic wash fraction obtained from bovine ROS membranes as previously characterized but without purifying the PDE6 beyond the initial hypotonic extraction (Goc et al., 2010). The protein concentration of the hypotonic fraction was roughly 10 mg/ml, and about one-third of the fraction was PDE6 (with the other two-thirds being the α and β subunits of transducin) (Supplemental Fig. 5). A 1:100 ratio of PDE6 fraction to buffer solution was allowed to incubate with or without inhibitors at 30°C in 96-well, black, chimney-style UV-Star UV-Transparent Microplates (Greiner Bio-One, Monroe, NC) for 10 minutes in the Flexstation 3 Benchtop Microplate Reader (Molecular Devices, Sunnyvale, CA). The reaction was then started by the addition of cGMP (Cayman Chemical, Ann Arbor, MI) and the reporting agent SNARF-1 (at 2 mM cGMP and 20 μM SNARF-1 final concentrations, respectively) to a final volume of 100 μL. Fluorescence excitation was at 514 nm, and dual emission wavelengths were set to 580 nm and 640 nm, with emission cutoff filters at 570 nm and 630 nm, respectively. The PDE6-catalyzed reaction was monitored every 30 seconds over 50 minutes at 30°C, and concentrations of each inhibitor spanned from 30 nM to 30 μM. Background fluorescence from wells containing only buffer and cGMP/SNARF-1 was subtracted from all samples, and group background from wells containing the highest concentration of each inhibitor in buffer plus cGMP/SNARF-1 in the absence of protein was also subtracted. All data were first normalized so that the reading at t = 0 minutes was set to 0 arbitrary units, and then the data from 580 nm were averaged with the absolute value of the data at 640 nm at each time point (they have an inverse relationship to decreasing pH). The average of the two emissions was used to limit fluorescence measurement artifacts. The data points were then normalized as a percentage of the saturated value for the reaction without inhibitors (black markers in Fig. 2). Three technical replicates were used for each condition, and the data are presented as mean ± S.D.

Ex Vivo ERG and Assessment of PDE6 Inhibition Constant. Female and male C57BL/6J mice at the age of 8–10 weeks were used in the ex vivo ERG experiments (n = 10 mice). The mice were dark-adapted overnight and sacrificed with CO_2 aspiration and cervical dislocation. Dissection of the eyes was executed under dim red light in a nutrition solution. The nutrition solution consisted of (in mM) Na^+, 133.4; K^+, 3.3; Mg^{2+}, 2.0; Ca^{2+}, 1.0; Cl^-, 142.7; glucose, 10.0; EDTA, 0.01; HEPES, 12.0; and Leibovitz culture medium L-15 (0.72 mg/ml). Immediately after sacrificing, the eyes were enucleated and cut open along the equator. The retina was segregated from the sclera. Subsequently, the retina was placed in a specimen holder [modified from Donner et al. (1988)] on a filter paper with photoreceptors directed upward. A continuous flow (5–6 ml/min) of nutrition solution perfused the retina on the photoreceptor side. The temperature of the solution was kept at 36.0 ± 0.5°C with a heat exchanger in contact with the specimen holder and a thermistor fixed near the retina.

K^+ currents of Müller glial cells were obstructed by utilizing 50 μM $BaCl_2$ (Bolnick et al., 1979; Nymark et al., 2005). Moreover, 20 μM of D,L-2-amino-4-phosphonobutyric acid, a group III metabotropic glutamate receptor agonist, was added into the solution to isolate the photoreceptor component of the ERG response (Vinberg et al., 2014). CB-5083 was dissolved in DMSO and added to the solution to achieve final concentrations of 31.3, 62.5, 93.8, or 125 nM. The control solution had the same concentration of DMSO as the solutions above but no CB-5083. The pH was set to 7.5 with NaOH. CB-5083 was obtained from MedChemExpress (Sollentuna, Sweden), and all other chemicals were from Merck Group/Sigma-Aldrich (Darmstadt, Germany). In previous studies, DMSO has been demonstrated to have a detrimental

effect on retinal function (Tsai et al., 2009; Galvao et al., 2014). In our experiments, however, the concentration of DMSO in the perfusion solution was 0.00026 v/v%, which is well below the safe level proposed for intravitreal injections in rats (0.1 v/v%) (Tsai et al., 2009). Supplemental Figure 6 shows the behavior of response latency in photoreceptoral ex vivo ERG. The addition of DMSO to the perfusion did not cause an observable change in the response kinetics.

The isolated dark-adapted retina was stimulated with homogenous full-field flashes of light with 1-millisecond exposure time from the photoreceptor side. A fiber-coupled LED (M530F2, Thorlabs Inc, NJ) with a nominal wavelength of 530 nm was employed to generate flashes of varying light intensity using a driver (DC2200, Thorlabs Inc, NJ). The homogeneity of the beam was confirmed with a camera-based beam profiler (model SP503U, Ophir-Spiricon Inc., Logan, UT). The dimmest stimulus strength was selected based on its ability to induce ~10% response amplitude compared with the saturation level. The subsequent stimuli in the series increased by 0.5-log-unit increments. The light power incident on the retina was measured with an optical power meter (PM100D, Thorlabs Sweden AB, Mölndal, Sweden). Light stimulus strengths were defined by calculating the number of photoisomerized rhodopsins per rod cell (R^*rod^{-1}) using the pigment template by Govardovskii et al. (2000), the emission spectrum of the LED, and the sensitivity spectrum of the optical power meter, as described before (Heikkinen et al., 2008). The stimulus strengths used in the experiments ranged from 6.0 to 2900 R^*rod^{-1}. Transretinal mass potential was recorded by two silver/silver chloride pellet electrodes (EP2, World Precision Instruments, Hitchin, UK) placed inside the solution-filled channels above and below the retina. The signal was amplified 1000×, low-pass-filtered (model 950 Bessel 8-pole filter, Frequency Devices Inc., IL; Low pass filter cut of frequency = 500 Hz), and sampled at 5 kHz (PCIe-6351; National Instruments, Austin, TX). The stimulus and recording devices were controlled with custom-made LabVIEW software on a PC. Photoreceptoral ERG responses were recorded from 17 retinas (n = 10 mice) both in control solution and in 1–2 different CB-5083 solutions per retina (10 retinas: one CB-5083 concentration; seven retinas: two CB-5083 concentrations). Different solutions were applied to the retina in the following order: control solution, CB-5083 concentration 1, control solution, CB-5083 concentration 2, and control solution. After each solution change, the ERG responses were allowed to stabilize 10–18 minutes before recording a set of responses for analysis.

The method for determination of a compound's inhibition constant for light-activated PDE6 via ex vivo ERG has been described in detail elsewhere (Turunen and Koskelainen, 2018). Briefly, the introduction of the PDE6 inhibitor compound to the retina leads to a decrease in the amplification of the phototransduction. This effect can be quantified by modeling the initial phase of the ERG responses with the activation model developed and described in detail by Pugh and Lamb (2000). Fitting the activation model equation (Turunen and Koskelainen, 2018, Eq. 6) to the response traces normalized to the saturation amplitude (Fig. 3B) enables the determination of amplification constant, A. The change in the amplification constant is dependent on the inhibition constant and the concentration of the inhibitor according to equation:

$$\frac{A_{control}}{A_{inhibitor}} = \frac{[I]}{K_{i,\,light}} + 1, \quad (1)$$

in which $A_{control}$ and $A_{inhibitor}$ are the amplification constants determined from the ERG responses recorded in control and inhibitor solutions, respectively, [I] is the concentration of the inhibitor in the perfusion solution, and $K_{i,light}$ is the inhibition constant of the inhibitor for light-activated PDE6. $A_{control}$ was determined here as the average of the amplification constants obtained in the control solution before and after the application of CB-5083. Plotting the relative amplification constant ($A_{control}/A_{inhibitor}$) as a function of inhibitor concentration and fitting a linear model enable the determination of the inhibition constant $K_{i,light}$ as the reciprocal of the slope. The relative change in response saturation amplitudes (Fig. 3A) was calculated by comparing the amplitude in the CB-5083 solution with the average of the corresponding amplitudes in the control solution (measured before and after application of CB-5083) to compensate for the gradual time-dependent decrease of ex vivo ERG response amplitudes. The analysis of the ERG responses was performed with Matlab 2020a (Mathworks Inc.).

Histology and Optical Coherence Tomography. Histology and optical coherence tomography (OCT) were performed as described earlier (Leinonen et al., 2019, 2020). OCT imaging using a Bioptigen spectral-domain OCT device (Leica Microsystems Inc., Buffalo Grove, IL) was performed after the in vivo ERG recordings while the animals were under the same anesthesia (vehicle-treated VCP mice, n = 5; CB-5083–treated VCP mice, n = 4; nontreated WT mice, n = 3). Briefly, four frames of OCT b-scan images were acquired from a series of 1200 a-scans. ONL thickness was measured 500 μm from the optic nerve head (ONH) at nasal, temporal, superior, and inferior quadrants. Finally, mice were subjected to terminal anesthesia and cervical dislocation. The superior side of the sclera/cornea was marked with a thread burner, and the eyes were enucleated and fixed in Hartman's fixative (Sigma-Aldrich, St. Louis, MO) for at least 24 hours and then transferred to 70% ethanol for short-term storage. Paraffin block preparation and sectioning at 10-μm thickness were ordered from Histowiz (Brooklyn, NY). Retinal panorama images were captured using a light microscope. Representative 40× magnified images shown in Fig. 4, L and M, were taken at the dorsal retina centered at ~800 μm from the ONH. IS/OS and ONL layer and whole retina thicknesses were measured at 500 μm distance from ONH both at the superior and inferior sides, and the superior-inferior average was used in Fig. 4N. Histology image morphometry was performed using ImageJ 1.52a software.

Statistical Analysis. We used a repeated-measures study design for the acute in vivo ERG experiments, wherein ERG responses after drug treatments were compared with each mouse's own baseline retinal function. Normality of the data was tested using the Shapiro-Wilk test and visually inspected from Q-Q plots. The acute in vivo ERG data were analyzed using two-way repeated-measures ANOVA. Group differences in ERG parameters and retinal thickness measurements from OCT images in long-term trials were analyzed by regular 2-way ANOVA. Treatment was set as the between-subjects factor and stimulus strength/retinal location as the within-subjects factor. Serum and tissue CB-5083 concentrations and retinal morphometry parameters in histology images were compared using one-way ANOVA. All ANOVAs that found a significant between-subjects effect or within-subjects/between subjects interaction effect were followed by Bonferroni's post hoc tests. The data are presented as mean ± S.D. and the level of statistical significance was set at $P < 0.05$.

Results

CB-5083 Suppresses Mouse Retinal Function In Vivo. PDE6 is an essential enzyme for energy transfer from the photons of visible light to electrical signals in our retinas known as phototransduction. These electrical signals can be readily recorded with a distant electrode inserted close to the eyelids (in humans) or in contact with the eye's cornea (in humans and animals) using a minimally invasive ERG method (Leinonen and Tanila, 2018). Any systemically administered experimental compound that crosses the physical barrier of the eye, the blood-retina barrier, and inhibits PDE6 may reduce the phototransduction amplification that is easily apparent in the ERG signal. Therefore, we began our investigation by recording scotopic (rod-photoreceptor dominant) and photopic (cone-photoreceptor specific) ERGs first after vehicle treatment (baseline) and then after acute CB-5083 administration in 1-week intervals using the same mice. These experiments were performed in healthy WT mice starting 45 minutes after treatments.

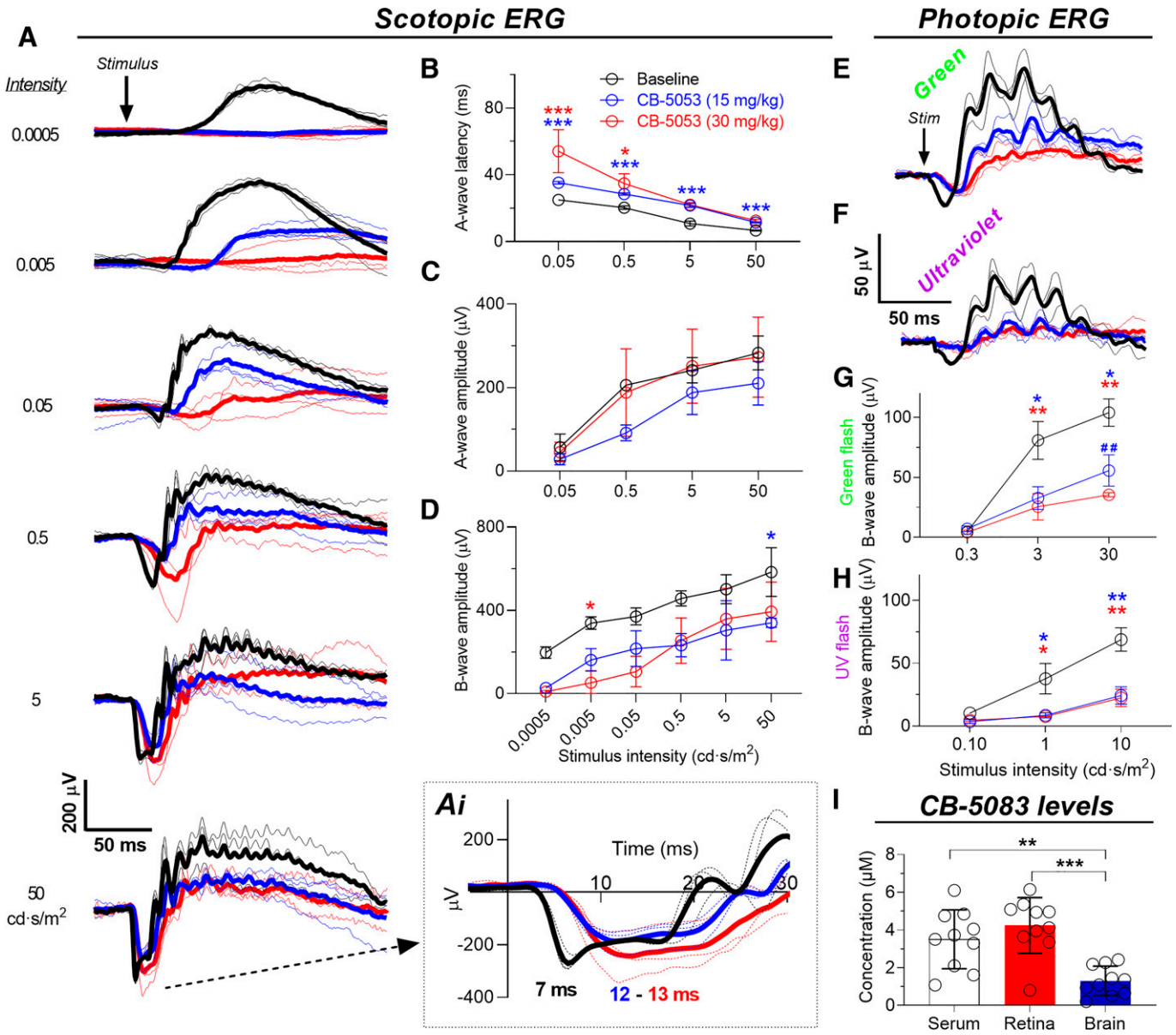

Fig. 1. Single administration of CB-5083 delays photoreceptor activation to light and suppresses retinal function. Electroretinograms (ERGs) were first recorded in nontreated C57BL/6J mice (baseline, $n = 3$, black) and then in separate sessions 45 minutes after CB-5083 gavage administration using doses of 15 mg/kg (blue, $n = 3$) and 30 mg/kg (red, $n = 3$), respectively. The sessions were separated by 1 week. Scotopic ERGs were recorded in fully dark-adapted mice. (A) Rod-dominant scotopic ERG waveforms. Thin traces are individual mouse responses, and thick lines are group averages. Inset Ai shows a magnified image of the A-wave leading edge at the highest stimulus strength and a-wave peak times. (B) A-wave latencies. (C) A-wave amplitudes. Repeated-measures ANOVA between-subjects main effect between baseline and 15 mg/kg CB-5083: $P < 0.01$. (D) B-wave amplitudes. (E and F) Photopic ERG waveforms in response to green (30 cd·s/m^2, peak wavelength 544 nm) and UV (10 cd·s/m^2, peak wavelength 365 nm) flashes stimulating the M- and S-cone photoreceptors, respectively. (G and H) Photopic ERG amplitudes. Statistical analysis: repeated-measures ANOVA followed by Bonferroni's post hoc tests. $^{*}P < 0.05$, $^{**/\#\#}P < 0.01$, $^{***}P < 0.001$. Asterisks mark significant difference between baseline and 15 mg/kg sildenafil (blue) or baseline and 30 mg/kg sildenafil (red). Pound signs in G mark difference between 15 mg/kg and 30 mg/kg sildenafil. ERG data are presented as mean ± S.D. (I) CB-5083 levels in mouse serum, retinae, and frontal cortex (brain) biopsy 1 hour after gavage administration ($n = 10$ in all). Statistical analysis: one-way ANOVA followed by Bonferroni's post hoc test: $^{**}P < 0.01$. Error bars denote S.D. Stim, stimulus.

CB-5083 decreased retinal sensitivity prominently at doses of 15 mg/kg and 30 mg/kg per mouse body weight (Fig. 1). Specifically, both dosing regimens completely abolished the ERG response to dim 0.0005 cd·s/m^2 light stimuli that cause a robust response under baseline nontreated conditions (Fig. 1A). With 1–2 log-units-higher light stimuli (0.005–0.05 cd·s/m^2), the ERG response started to recover characteristic waveform appearance after administration of 15 mg/kg CB-5083, but it was still significantly distorted after the 30 mg/kg dose. Quantitative measurements of ERG a-wave latency (Fig. 1B) and amplitude (Fig. 1C) and b-wave amplitude (Fig. 1D) confirmed the significance of the effect. Among these parameters, the a-wave latency most reliably defines the drug effect on phototransduction. The modified scotopic ERG wave form caused by impaired phototransduction renders amplitude comparisons to the healthy/normal waveform less reliable.

Recordings in the photopic condition (Fig. 1, E–H), in which flash stimuli are superimposed on a steady rod-suppressing background, revealed that CB-5083 might desensitize cone function, especially the UV-selective cone function in mice (Fig. 1, F and H), even more so than the rod function.

Since patients' complaints of visual disturbance in the previous phase 1 clinical trial with CB-5083 were similar to those occasionally occurring in association with erectile-dysfunction drug usage, we were interested in recording ERGs after systemic administration of vardenafil, sildenafil, or tadalafil to see how their effects compared with those of CB-5083. Among these widely used clinical medications, vardenafil caused a robust dose-dependent suppression of phototransduction (Supplemental Fig. 1). With a dose of 30 mg/kg, the effect of vardenafil appears to be even stronger than that of CB-5083, as this dose of vardenafil practically fully suppressed the cone function in mice. The same dose of sildenafil and tadalafil moderately but less than CB-5083 suppressed retinal function in mice (Supplemental Figs. 2 and 3). The erectile-dysfunction drugs are designed to target PDE5, but they display off-target effects on PDE6, which results in the observed effects on phototransduction (Moschos and Nitoda, 2016; Yafi et al., 2018). We similarly tested the effects of systemic administration of the PDE6-selective experimental compound zaprinast; however, it did not significantly affect phototransduction at a 30 mg/kg dose (Supplemental Fig. 4).

CB-5083 Reaches a High Concentration in the Mouse Retina after an Acute Gavage Administration. We next determined to what extent CB-5083 reaches the retina and the molar ratio between the circulating and retinal levels of the drug. We performed CB-5083 administration by gavage into mice similarly as before the acute in vivo ERG experiments. To match the timing to what would be roughly halfway through the ERG experiment, we collected blood and tissue samples 1 hour after drug administration. Liquid chromatography–mass spectrometry analysis showed high drug concentrations in both the mouse serum and retinae (Fig. 1I). In fact, the molar CB-5083 concentrations in the mouse serum and in the perfused retinae were nearly identical, indicating that CB-5083 may freely cross the blood-retina barrier. To inspect CB-5083 levels in another neuronal tissue, we collected and analyzed frontal cortex biopsies. CB-5083 concentration in this brain region was ~3-fold lower compared with serum and retinae (Fig. 1I).

CB-5083 Is a Potent Inhibitor of PDE6 in Bovine ROS Extracts. To test the hypothesis that CB-5083 targets PDE6, we performed a previously characterized PDE6-activity assay in bovine ROS (Baker and Palczewski, 2011). Consistent with our observations from acute in vivo ERG experiments (Fig. 1; Supplemental Figs. 1 and 2), we found that CB-5083's inhibitory potency on PDE6 is between those of sildenafil and vardenafil (Fig. 2). From the dosages we tested, sildenafil started to inhibit cGMP hydrolysis at 3 μM, whereas CB-5083 and vardenafil showed some inhibitory effect already at 0.03 μM concentration (Fig. 2A). At 3 μM concentration, vardenafil strongly inhibited cGMP hydrolysis, whereas CB-5083 had a moderate effect (Fig. 2C). With the largest dose tested, 30 μM (Fig. 2D), vardenafil and CB-5083, to a slightly lesser extent, almost completely blocked cGMP hydrolysis during the 50-minute experiment. Our assay using ROS extracts rather than purified PDE6 did not allow inspection of precise dose-response relationships or determination of IC_{50} values.

CB-5083 Displays a Dose-Dependent but Reversible Inhibition on Phototransduction in Mouse Retinas Ex Vivo. Our analysis of CB-5083 levels in the mouse serum and retina show that CB-5083 readily enters the retina from the systemic circulation. Furthermore, our in vivo ERG recordings indicate that CB-5083 suppresses retinal function by inhibiting phototransduction, and our biochemical assay of bovine ROS extracts confirmed robust PDE6 inhibition. To investigate dose dependence and inhibition reversibility of CB-5083, we recorded photoreceptoral ex vivo ERG from isolated and perfused mouse retinae. The photoreceptor component of the ERG was obtained by adding $BaCl_2$ and D,L-2-amino-4-phosphonobutyric acid to the perfusion.

Figure 3A presents two sets of scotopic ex vivo ERG responses from a single retina to increasing flash stimuli. Black traces represent responses recorded in control solution, and orange traces were recorded in the solution containing 125 nM CB-5083. CB-5083 at 125 nM concentration elevated the response saturation amplitude by 36 ± 14% (n = 6, mean ± S.D.). The increase in amplitude indicates that CB-5083 decreases the basal hydrolytic activity of PDE6 in photoreceptors, which induces an increase in the intracellular cGMP concentration and, thus, in the ERG saturation amplitude (Turunen and Koskelainen, 2018; Rieke and Baylor, 1996). Notably, the increase in saturation level amplitude was not observed in the in vivo ERG recording (Fig. 1, A and C) because in these recordings synaptic transmission to second-order neurons (seen as positive polarity b-wave) limited this phenomenon. Additionally, CB-5083 slowed down the leading edge of the responses and delayed response

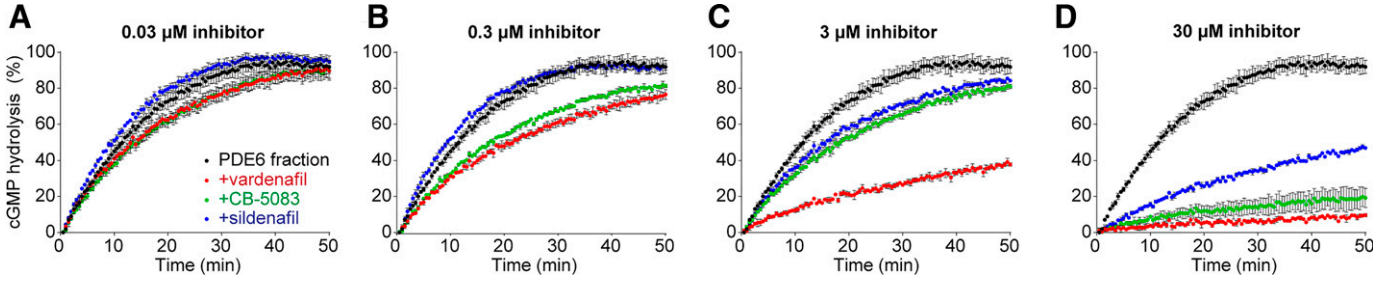

Fig. 2. CB-5083 inhibits PDE6-mediated cGMP hydrolysis. (A–D) PDE6-mediated cGMP hydrolysis in the absence or presence of vardenafil (red), CB-5083 (green), or sildenafil (blue), with doses ranging from 30 nM to 30 μM. Three technical replicates were performed per condition. Data are plotted as mean ± S.D.

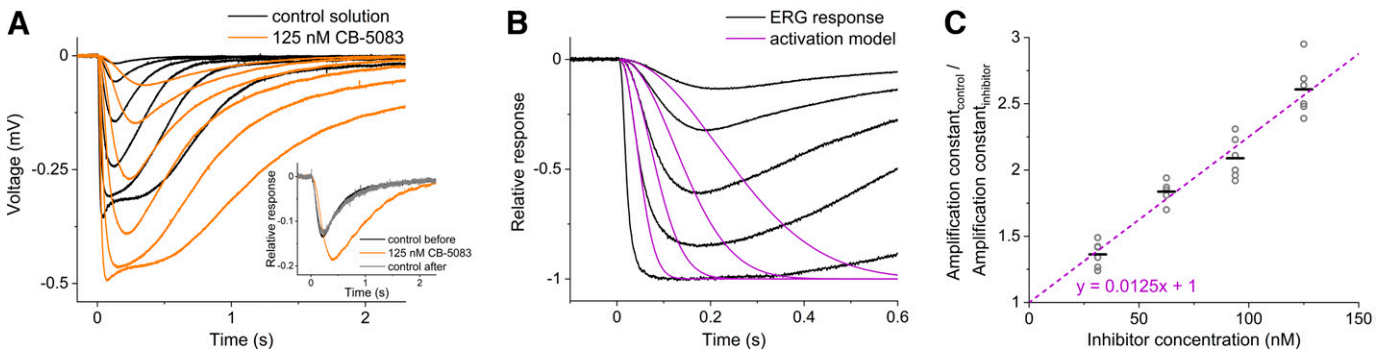

Fig. 3. CB-5083 dose-dependently and reversibly inhibits phototransduction in mouse retinas ex vivo. (A) The effect of CB-5083 on photoreceptoral ERG responses of isolated retinae. The responses were recorded with increasing stimulus strengths for retinae in control solution (black traces) and in 125 nM CB-5083 (orange traces). Each response trace is averaged from 1–5 repetitions with the same stimulus strength. The stimulus strengths (in R^*rod^{-1}) were 6.0, 18, 60, 180, 600, and 1800 for both solutions. The data are from a single representative retina. Inset: a response to the same dim flash stimulus for the retina in control solution (black trace), for the retina in 125 nM CB-5083 (orange trace), and for the treated retina in control solution after washout of CB-5083 (gray trace) to demonstrate reversibility. The stimulus strength was 7.2 R^*rod^{-1} in all solutions. The responses are normalized to the saturation amplitude, which indicates the complete suppression of the photoreceptor dark current (Turunen and Koskelainen, 2017). The data are from a single representative retina. (B) Fitting of the activation model (purple traces) to a set of subsaturated photoreceptoral ERG responses (black traces). (C) Determination of the CB-5083 inhibition constant. Photoreceptoral ERG responses were recorded from 17 retinas both in control solution and in 1–2 different CB-5083 solutions per retina. The CB-5083 concentrations were 31.3, 62.5, 93.8, and 125 nM. Each concentration was studied $n = 6$ times in total with different retinas to constitute the dataset of relative amplification constant ($A_{control}/A_{inhibitor}$) as a function of inhibitor concentration (gray circles). The slope of the linear fit to the data is 0.0125 nM^{-1} (purple dashed trace), corresponding to the inhibition constant of $K_i = 80 \pm 3$ nM (S.E.). The black horizontal lines indicate the mean.

return to the baseline. The slowdown of the response leading edge is consistent with a decrease in phototransduction amplification due to diminished PDE6 catalytic activity. The delayed response return to baseline suggests decreased turnover rate of cGMP, which is a consequence of decreased basal PDE6 activity (Pugh and Lamb, 2000). The amplitude increase, the deceleration of response leading edge, and the delayed response return to the baseline are all consistent with the interpretation that CB-5083 targets PDE6 in photoreceptors. Figure 3A inset illustrates the reversibility of the CB-5083 effect by showing representative normalized ERG responses to dim flashes of light for a retina in control solution (black trace), in 125 nM CB-5083 solution (orange trace), and again in control solution after the washout of CB-5083 (gray trace). The responses showed either full or nearly complete recovery after the reintroduction of the control solution.

To quantify the potency of CB-5083, we used a recently established ex vivo ERG-based method, enabling the determination of a compound's inhibition constant (K_i) against PDE6 in native conditions (Turunen and Koskelainen, 2018). In this method, the inhibitor compound is introduced to the retina, causing a decrease in PDE6 catalytic activity and thus a reduction in the molecular amplification of phototransduction. The effect is quantified by analyzing the initial phase of the ERG signal in the theoretical framework of the phototransduction activation model developed by Pugh and Lamb (1992). We fitted the activation model to the leading edges of photoresponses recorded from 17 retinas in four different CB-5083 concentrations and in the control solution (Fig. 3B). The relative amplification constant was directly proportional to inhibitor concentration (Fig. 3C), which is consistent with Eq. 1 and illustrates the dose-dependent effect of CB-5083 on photoreceptor function. Accordingly, the inhibition constant K_i against PDE6 was calculated as the reciprocal of the slope of the linear fit of the data points, leading to a value of $K_i = 80$ nM, which is 7-fold smaller compared with the K_i obtained for sildenafil previously using the same method (Turunen and Koskelainen, 2018).

Retinal Function Recovers after Treatment Cessation and No Ocular Abnormalities Are Observed after Chronic CB-5083 Treatment in Middle-Aged VCP-Disease Model Mice. The strong dependence of phototransduction suppression on CB-5083 concentration indicates that its clinical application in VCP disease could be feasible after dose titration regardless of off-target effects on PDE6. However, this assertion requires that CB-5083's negative effects on visual function be reversible and that function recover to normal if unacceptable side effects occur. In addition, chronic retinal toxicity needs to be ruled out.

To assess the long-term ocular safety of chronic CB-5083 usage, we used middle-aged heterozygous VCP^{R155H} knock-in mice. We dosed the mice via daily gavage (CB-5083, 15 mg/kg) for 6 months, over the period from 12 months of age to 18 months. An equal number of the mice were dosed in parallel with the same volume of vehicle to serve as controls. After the 6-month treatment, we recorded ERGs after a 24-hour period from the last administration to avoid the acute effects of CB-5083 on phototransduction. At 18 months of age, both A- and B-wave amplitudes in vehicle-treated VCP mice were slightly smaller compared with age-matched, nontreated WT mice (Fig. 4, B and D; 2-way ANOVA between-subjects effects: A-wave, $F_{1,6} = 6.10$, $P < 0.05$; B-wave, $F_{1,6} = 12.4$, $P < 0.05$). This could be an effect of long-term vehicle treatment or related to mouse genetic background (not littermates), as we later recorded nontreated 24-month-old heterozygous VCP and slightly younger WT mice (19-month-old) and did not find statistically significant differences between them (Supplemental Fig. 7). Therefore, it seems unlikely that the heterozygous VCP^{R155H} knock-in mutation deleteriously affects visual function. Importantly, our results from drug-treated mice show that the negative effects of CB-5083 on phototransduction are reversible, and visual function in mice recovers virtually to WT levels already after

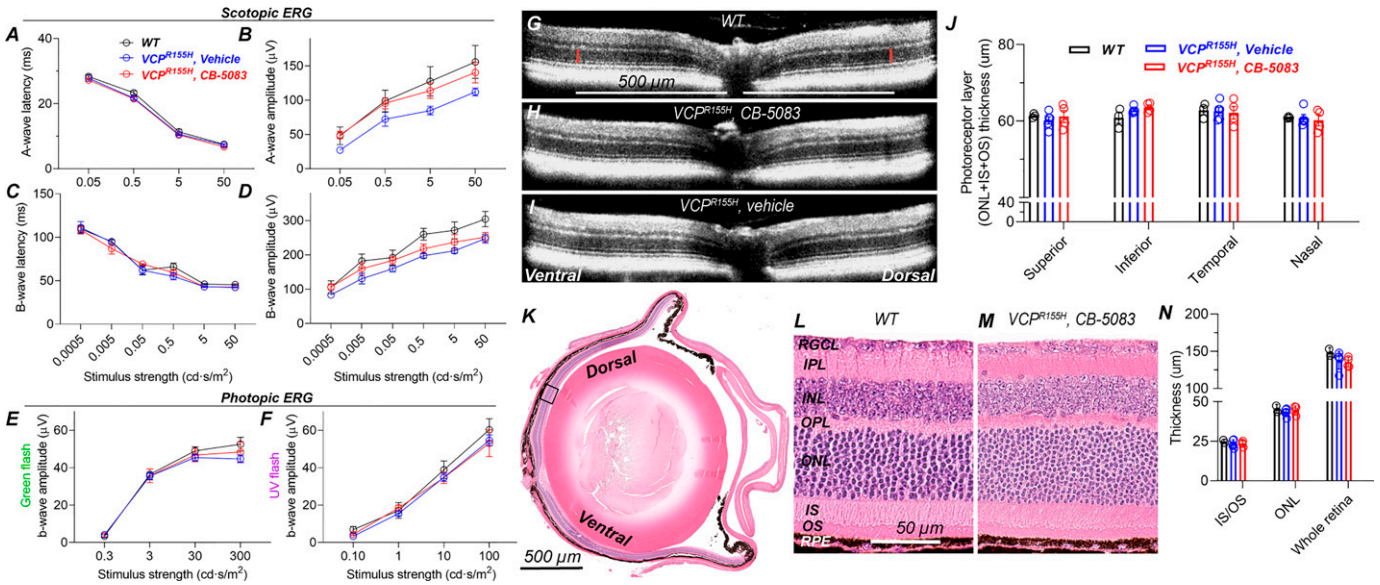

Fig. 4. Chronic use of CB-5083 is safe for the eyes, and visual function recovers after drug washout. VCP-disease mice (*VCP*^{R155H} knock-in heterozygous mutants) were treated daily with CB-5083 (n = 4, 15 mg/kg) or with vehicle (controls, n = 5) by gavage for 6 months between 12 and 18 months of age. Eighteen-month-old, healthy, and nontreated C57BL/6J mice were used as a WT control (n = 3). At the end of the trial, ERG and OCT were conducted 24 hours after the last dose. (A and C) Scotopic ERG A- and B-wave latency analyses indicate no difference in phototransduction or photoreceptor-to-bipolar cell synaptic transmission speed, respectively, between the study groups. Instead, scotopic ERG amplitude analyses (B and D) indicate moderately but statistically significantly lower A- and B-wave amplitudes for vehicle-treated VCP mice compared with nontreated healthy controls (2-way ANOVA between-subjects main effects in both: $P < 0.05$). CB-5083–treated VCP mice had slightly higher B-wave amplitudes compared with vehicle-treated VCP mice (ANOVA between-subjects: $P < 0.05$). (E and F) Photopic ERG amplitudes did not differ between study groups. (G–I) Representative OCT images from WT (G), CB-5083–treated (H), and vehicle-treated (I) VCP-disease mice. (J) Photoreceptor thickness is equal among the three study groups. (K) Representative histologic WT mouse eye section for illustration. The black box indicates the area where 40× images (L and M) were acquired. (L and M) High-magnification images show similar morphology in the nontreated WT and chronically CB-5083–treated VCP-disease mouse retinas. (N) IS/OS, ONL, and whole retina thickness measurements from histology images (n for CB-5083–treated same as above, but n = 2 for WT). INL, inner nuclear layer; IPL, inner plexiform layer; OPL, outer plexiform layer; RGCL, retinal ganglion cell layer; RPE, retinal pigment epithelium. All graphs show mean ± S.D., and retinal thickness layer analyses also show individual replicates. Statistical comparison was performed using 2-way (ERG and OCT) or 1-way ANOVA (histology).

a 24-hour washout despite many months of continuous treatment (Fig. 4, A–F). After drug washout, we did detect a small but statistically significant *increase* in a-wave amplitude in CB-5083–treated versus vehicle-treated VCP mice (Fig. 4B; 2-way ANOVA between-subjects effect: $F_{1,7} = 6.57$, $P < 0.05$). We interpret that this result could be either a type 1 error, or it could be a neural rebound effect after the 6-month-long partial phototransduction suppression by PDE6 inhibition. However, further investigation of this phenomenon was beyond the scope of the current study.

Since CB-5083 has an off-target inhibitory effect on PDE6 that is most abundantly expressed in the photoreceptors, they would be the locus at which long-term ocular toxicity would most likely occur. The thickness of the outer retina (photoreceptor nuclei and photoreceptor ciliary segments) is an established measure of photoreceptor toxicity and can be reproducibly measured with noninvasive OCT imaging (Marmor, 2012). Therefore, we performed OCT after the 6-month-long trial in WT and VCP-disease mice. We did not detect any obvious abnormalities in the OCT images (Fig. 4, G–I) nor did we find differences in photoreceptor layer thickness among the study groups (Fig. 4J). Furthermore, a more high-resolution inspection from histologic retinal sections did not reveal abnormalities to retinal structure after chronic CB-5083 treatment (Fig. 4, L and M) or alterations in photoreceptor inner + outer segment, photoreceptor nuclei layer, or whole retina thickness (Fig. 4N), consistent with the recovered retinal function.

Discussion

VCP disease is a rare genetic disorder caused by missense gain-of-function mutations in the *VCP* gene (Watts et al., 2004). One report estimated its prevalence in the United Kingdom at 0.66 per million (Figueroa-Bonaparte et al., 2016). Nevertheless, the disease is devastating for the patients and their families. No curative therapies exist for these conditions, and because of their rarity, the major pharmaceutical industry is unlikely to pursue extensive research efforts. Typically, with respect to rare genetic disorders, such as VCP disease, it is up to the academic community, patient advocate groups, small pharmaceutical/biotech companies, individual venture capitalists and/or philanthropists to make the effort and investment to discover prospective pharmacotherapies. One potential pharmacotherapy is the CB-5083 compound that was originally developed to drive cytotoxic cellular responses in cancer (Le Moigne et al., 2017). Given the gain-of-function mechanisms of VCP-disease–causing mutations, CB-5083 could potentially be repurposed for the treatment of neurodegenerative VCP disorders, wherein it could be used to normalize aberrantly elevated activity. The option of drug repurposing is attractive, as major preclinical evaluations of CB-5083 have already been conducted, and its general safety was documented in the recent phase 1 clinical trial. However, the clinical trial in cancer patients was halted because of CB-5083's adverse effects on vision.

Since the documented side effects of CB-5083 closely resemble those observed in association with usage of erectile-dysfunction drugs (Yafi et al., 2018; Moschos and Nitoda, 2016), we hypothesized that they share the same mechanism. The erectile-dysfunction drugs vardenafil, sildenafil, and tadalafil are designed to selectively inhibit the PDE5 enzyme; however, especially vardenafil and sildenafil also inhibit PDE6 as an off-target effect (Zhang et al., 2005; Hatzimouratidis et al., 2016). As PDE6 is an essential enzyme in phototransduction in our photoreceptors, the severity of the side effect on vision depends on the drug's distribution properties from the blood circulation to the eye and on its inhibitory potency for PDE6, which can be described by the inhibition constant. Our investigation of CB-5083 concentration from mouse serum and retinae revealed that the drug crosses the blood-retina barrier essentially without resistance so that the retinal drug level and the circulatory drug level were nearly the same after acute administration (Fig. 1I). Our ERG recordings in WT mice after acute CB-5083 dosing showed that the drug significantly desensitized retinal function (Fig. 1, A–H). It particularly delayed the photoreceptor response (increased scotopic a-wave latency), which is consistent with the hypothesis of direct PDE6 inhibition (Turunen and Koskelainen, 2018). We recorded similar ERGs after acute administration of vardenafil (Supplemental Fig. 1), sildenafil (Supplemental Fig. 2), and tadalafil (Supplemental Fig. 3); only vardenafil affected retinal function as much or more than CB-5083 (Fig. 1; Supplemental Fig. 1). Sildenafil and tadalafil had only a moderate phototransduction-suppressive effect with the relatively large dose of 30 mg/kg per mouse body weight (Supplemental Figs. 2 and 3). Interestingly, an experimental compound, zaprinast, a relatively selective PDE6 inhibitor with K_i against PDE6 of 30 nM (10-fold selectivity for PDE6 compared with closely related PDE5) (Zhang et al., 2005), did not have any significant effects on the ERG signal (Supplemental Fig. 4). This result indicates that zaprinast may not enter the eye from the circulation and reach a sufficient concentration to affect photoreceptor function.

To directly assess CB-5083's inhibitory action on PDE6, we used a well characterized PDE6-activity assay (Baker and Palczewski, 2011) using bovine ROS extracts. We found that treating the ROS extracts with CB-5083, sildenafil, or vardenafil significantly slowed the rate of cGMP hydrolysis, a reaction driven by PDE6 in this system. Specifically, at a dose of 30 μM for each drug, vardenafil and CB-5083 nearly abolished cGMP hydrolysis, whereas sildenafil significantly decreased the hydrolysis rate but to a much lesser extent during the 50-minute experiment. The relative dose dependence of the three drugs showed their order of inhibitory potency for PDE6 as vardenafil > CB-5083 > sildenafil. These results are in good agreement with our findings from in vivo ERG experiment and ex vivo ERG experiments (Figs. 1 and 3; Supplemental Figs. 1 and 2). Altogether, our results for the known PDE inhibitors are in line with published affinity data, as Ki-values of 0.71 nM, 11 nM, and 21 μM for PDE6 have been determined against trypsin-activated purified bovine rod PDE6 for vardenafil, sildenafil, and tadalafil (tadalafil was not tested in our PDE6-activity assay), respectively (Zhang et al., 2005).

Knowing the PDE6 inhibition constant (K_i) of CB-5083 and comparing it to a clinically used drug would increase confidence for its clinical translation. Furthermore, it is important to document the dose-response relationship of the drug for suppression of photoreceptor function and to ascertain whether the effect is reversible after drug washout. A K_i value of 560 nM for sildenafil was recently determined for light-activated mouse PDE6 under its native conditions without biochemical manipulations, using a novel electrophysiology-based method (Turunen and Koskelainen, 2018). We used the same method and setup to investigate the inhibitory potency of CB-5083. Our K_i value of 80 nM for CB-5083 (Fig. 3) shows it to be a 7-fold more potent inhibitor of light-activated PDE6 than sildenafil. CB-5083's dose-response relationship for phototransduction suppression followed the relation

$$A_{inhibitor} = \frac{A_{control}}{1 + \frac{[I]}{K_{i,\,light}}} \quad (2)$$

(a nonlinearized form of Eq. 1), with concentrations up to 125 nM in intact mouse retinas (Fig. 3). These results indicate that the clinical side effects of CB-5083 on vision are likely to be directly dose-dependent in a regular and predictable fashion.

Typically, the drug doses needed to suppress tumor growth in cancer therapy are significantly higher than needed for therapeutic efficacy in other indications, such as in autoimmune diseases (Liu et al., 2011). Accordingly, we hypothesize that a lower dose of CB-5083 could be effective in VCP disease than that used in the previous phase 1 cancer trial, resulting in milder side effects on visual function. Still, as CB-5083 is a potent inhibitor of PDE6, side effects in some patients are practically unavoidable. Nevertheless, if the side effects are transient and vision returns to normal after cessation of drug use, those patients that tolerate the drug could use it safely. Therefore, we finally performed a long-term (6-month) ocular safety trial in WT and VCP-disease model mice. We chose the VCP-disease model mice to increase the reliability and translational potential of the results. A potential rare gene-drug interactions would not be detected in a WT genotype but could arise in the disease model mice. The usage of middle-aged mice further increases translational significance, as VCP disease is typically diagnosed in humans around middle age (Kimonis et al., 2008), and these patients would likely constitute the population in prospective clinical trials. After a 24-hour washout period after 6-month-long daily CB-5083 administration, the ERG signal practically recovers to normal (Fig. 4). We also did not observe any abnormalities in retinal macrostructure by OCT imaging or standard histology. Retinal ONL thickness, an established and sensitive marker of photoreceptor toxicity (Marmor, 2012), was the same among all study groups as assessed by two distinct methods. Taken together, our data show that CB-5083 dose-dependently inhibits PDE6, causing a reduction of phototransduction amplification that results in visual dysfunction. However, this effect is reversible and disappears shortly after drug use is ended.

Finally, even though the visual side effects of vardenafil and sildenafil are relatively common, millions of people have used them safely for decades (Yafi et al., 2018). The use of these drugs in erectile dysfunction is typically intermittent, but low-dose sildenafil is also used daily in the treatment of pulmonary arterial hypertension (Rubin et al., 2011). Concern has been raised from reports associating PDE5 inhibitor drugs with permanent toxic effects on the retina/visual function, particularly in the form of a rare nonarteritic ischemic optic neuropathy (Moschos and Nitoda, 2016; Yafi et al., 2018). A few large case-crossover studies concluded that the weekly use of

PDE5 inhibitors may double the risk of acute nonarteritic ischemic optic neuropathy (Campbell et al., 2015; Flahavan et al., 2017), whereas a large meta-analysis covering nearly a million PDE5-inhibitor users found no significantly increased risk (Liu et al., 2018). Currently, consensus prevails that clinical PDE5 inhibitors do not considerably increase the risk of permanent toxic effects on chorioretinal tissue, photoreceptors, or vision at clinical doses (Zoumalan et al., 2009; Moschos and Nitoda, 2016; Yafi et al., 2018). However, as always with pharmacotherapy, the potential risks still need to be weighed with the benefits.

In conclusion, our data suggest that repurposing CB-5083 for the treatment of VCP disease or other applicable conditions is a viable option with respect to drug safety, as lowering drug doses would decrease the occurrence and severity of visual side effects. In addition, according to our data from mice, these side effects are transient and do not cause permanent ocular toxicity. Finally, regarding drug research and development in general, we recommend adding in vivo and/or ex vivo ERG recordings as an economic and efficient method to screen drug effects on PDEs and neurotransmission.

Authorship Contributions

Participated in research design: Leinonen, Cheng, Pitkänen, Sander, Turunen.

Conducted experiments: Leinonen, Cheng, Pitkänen, Sander, Zhang, Saeid, Weiss, Ta, Ton.

Contributed new reagents or analytic tools: Koskelainen, Vargas, Kimonis, Palczewski.

Performed data analysis: Leinonen, Pitkänen, Sander, Zhang, Turunen.

Wrote or contributed to the writing of the manuscript: Leinonen, Cheng, Pitkänen, Sander, Zhang, Saeid, Turunen, Vargas, Kimonis, Palczewski.

References

Anderson DJ, Le Moigne R, Djakovic S, Kumar B, Rice J, Wong S, Wang J, Yao B, Valle E, Kiss von Soly S, et al. (2015) Targeting the AAA ATPase p97 as an approach to treat cancer through disruption of protein homeostasis. *Cancer Cell* **28**:653–665.

Badadani M, Nalbandian A, Watts GD, Vesa J, Kitazawa M, Su H, Tanaja J, Dec E, Wallace DC, Mukherjee J, et al. (2010) VCP associated inclusion body myopathy and paget disease of bone knock-in mouse model exhibits tissue pathology typical of human disease. *PLoS One* **5**:e13183 10.1371/journal.pone.0013183.

Baker BY and Palczewski K (2011) Detergents stabilize the conformation of phosphodiesterase 6. *Biochemistry* **50**:9520–9531.

Blythe EE, Olson KC, Chau V, and Deshaies RJ (2017) Ubiquitin- and ATP-dependent unfoldase activity of P97/VCP•NPLOC4•UFD1L is enhanced by a mutation that causes multisystem proteinopathy. *Proc Natl Acad Sci USA* **114**:E4380–E4388.

Bolnick DA, Walter AE, and Sillman AJ (1979) Barium suppresses slow PIII in perfused bullfrog retina. *Vision Res* **19**:1117–1119.

Campbell UB, Walker AM, Gaffney M, Petronis KR, Creanga D, Quinn S, Klein BE, Laties AM, Lewis M, Sharlip ID, et al. (2015) Acute nonarteritic anterior ischemic optic neuropathy and exposure to phosphodiesterase type 5 inhibitors. *J Sex Med* **12**:139–151.

Donner K, Hemilä S, and Koskelainen A (1988) Temperature-dependence of rod photoresponses from the aspartate-treated retina of the frog (Rana temporaria). *Acta Physiol Scand* **134**:535–541.

Figueroa-Bonaparte S, Hudson J, Barresi R, Polvikoski T, Williams T, Töpf A, Harris E, Hilton-Jones D, Petty R, Willis TA, et al. (2016) Mutational spectrum and phenotypic variability of VCP-related neurological disease in the UK. *J Neurol Neurosurg Psychiatry* **87**:680–681.

Flahavan EM, Li H, Gupte-Singh K, Rizk RT, Ruff DD, Francis JL, and Kinchen KS (2017) Prospective case-crossover study investigating the possible association between nonarteritic anterior ischemic optic neuropathy and phosphodiesterase type 5 inhibitor exposure. *Urology* **105**:76–84.

Galvao J, Davis B, Tilley M, Normando E, Duchen MR, and Cordeiro MF (2014) Unexpected low-dose toxicity of the universal solvent DMSO. *FASEB J* **28**:1317–1330.

Goc A, Chami M, Lodowski DT, Bosshart P, Moiseenkova-Bell V, Baehr W, Engel A, and Palczewski K (2010) Structural characterization of the rod cGMP phosphodiesterase 6. *J Mol Biol* **401**:363–373.

Govardovskii VI, Fyhrquist N, Reuter T, Kuzmin DG, and Donner K (2000) In search of the visual pigment template. *Vis Neurosci* **17**:509–528.

Hatzimouratidis K, Salonia A, Adaikan G, Buvat J, Carrier S, El-Meliegy A, McCullough A, Torres LO, and Khera M (2016) Pharmacotherapy for erectile dysfunction: Recommendations from the Fourth International Consultation for Sexual Medicine (ICSM 2015). *J Sex Med* **13**:465–488.

Heikkinen H, Nymark S, and Koskelainen A (2008) Mouse cone photoresponses obtained with electroretinogram from the isolated retina. *Vision Res* **48**:264–272.

Kimonis VE, Fulchiero E, Vesa J, and Watts G (2008) VCP disease associated with myopathy, Paget disease of bone and frontotemporal dementia: review of a unique disorder. *Biochim Biophys Acta* **1782**:744–748.

Lamb TD and Pugh Jr EN (1992) A quantitative account of the activation steps involved in phototransduction in amphibian photoreceptors. *J Physiol* **449**:719–758.

Leinonen H, Choi EH, Gardella A, Kefalov VJ, and Palczewski K (2019) A mixture of U.S. Food and Drug Administration-approved monoaminergic drugs protects the retina from light damage in diverse models of night blindness. *Invest Ophthalmol Vis Sci* **60**:1442–1453.

Leinonen H, Pham NC, Boyd T, Santoso J, Palczewski K, and Vinberg F (2020) Homeostatic plasticity in the retina is associated with maintenance of night vision during retinal degenerative disease. *eLife* **9**:E59422 10.7554/eLife.59422.

Leinonen H and Tanila H (2018) Vision in laboratory rodents-Tools to measure it and implications for behavioral research. *Behav Brain Res* **352**:172–182.

Le Moigne R, Aftab BT, Djakovic S, Dhimolea E, Valle E, Murnane M, King EM, Soriano F, Menon MK, Wu ZY, et al. (2017) The p97 inhibitor CB-5083 is a unique disrupter of protein homeostasis in models of multiple myeloma. *Mol Cancer Ther* **16**:2375–2386.

Liu B, Zhu L, Zhong J, Zeng G, and Deng T (2018) The association between phosphodiesterase type 5 inhibitor use and risk of non-arteritic anterior ischemic optic neuropathy: A systematic review and meta-analysis. *Sex Med* **6**:185–192.

Liu J, Zhao J, Hu L, Cao Y, and Huang B (2011) Low dosages: new chemotherapeutic weapons on the battlefield of immune-related disease. *Cell Mol Immunol* **8**:289–295.

Marmor MF (2012) Comparison of screening procedures in hydroxychloroquine toxicity. *Arch Ophthalmol* **130**:461–469.

Moschos MM and Nitoda E (2016) Pathophysiology of visual disorders induced by phosphodiesterase inhibitors in the treatment of erectile dysfunction. *Drug Des Devel Ther* **8**:3407–3413.

Nalbandian A, Llewellyn KJ, Kitazawa M, Yin HZ, Badadani M, Khanlou N, Edwards R, Nguyen C, Mukherjee J, Mozaffar T, et al. (2012) The homozygote VCP(R(1)(5)(5)H/R(1)(5)(5)H) mouse model exhibits accelerated human VCP-associated disease pathology. *PLoS One* **7**:e46308 10.1371/journal.pone.0046308.

Nikonov SS, Kholodenko R, Lem J, and Pugh Jr EN (2006) Physiological features of the S- and M-cone photoreceptors of wild-type mice from single-cell recordings. *J Gen Physiol* **127**:359–374.

Nymark S, Heikkinen H, Haldin C, Donner K, and Koskelainen A (2005) Light responses and light adaptation in rat retinal rods at different temperatures. *J Physiol* **567**:923–938.

Orban T, Leinonen H, Getter T, Dong Z, Sun W, Gao S, Veenstra A, Heidari-Torkabadi H, Kern TS, Kiser PD, et al. (2018) A combination of G protein-coupled receptor modulators protects photoreceptors from degeneration. *J Pharmacol Exp Ther* **364**:207–220.

Pugh EN and Lamb TD (2000) Phototransduction in vertebrate rods and cones: Molecular mechanisms of amplification, recovery and light adaptation, in *Handbook of Biological Physics*, chap 5. Stavenga DG, DeGrip WJ, and Pugh EN, eds) pp 183–255, North-Holland.

Rieke F and Baylor DA (1996) Molecular origin of continuous dark noise in rod photoreceptors. *Biophys J* **71**:2553–2572.

Rubin LJ, Badesch DB, Fleming TR, Galiè N, Simonneau G, Ghofrani HA, Oakes M, Layton G, Serdarevic-Pehar M, McLaughlin VV, et al.; SUPER-2 Study Group (2011) Long-term treatment with sildenafil citrate in pulmonary arterial hypertension: the SUPER-2 study. *Chest* **140**:1274–1283.

Song C, Wang Q, and Li CC (2003) ATPase activity of p97-valosin-containing protein (VCP). D2 mediates the major enzyme activity, and D1 contributes to the heat-induced activity. *J Biol Chem* **278**:3648–3655.

Tsai TI, Bui BV, and Vingrys AJ (2009) Dimethyl sulphoxide dose-response on rat retinal function. *Doc Ophthalmol* **119**:199–207.

Tsujimoto Y, Tomita Y, Hoshida Y, Kono T, Oka T, Yamamoto S, Nonomura N, Okuyama A, and Aozasa K (2004) Elevated expression of valosin-containing protein (p97) is associated with poor prognosis of prostate cancer. *Clin Cancer Res* **10**:3007–3012.

Turunen TT and Koskelainen A (2017) Transretinal ERG in studying mouse rod phototransduction: Comparison with local ERG across the rod outer segments. *Invest Ophthalmol Vis Sci* **58**:6133–6145.

Turunen TT and Koskelainen A (2018) Electrophysiological determination of phosphodiesterase-6 inhibitor inhibition constants in intact mouse retina. *Toxicol Appl Pharmacol* **345**:57–65.

Vinberg F, Kolesnikov AV, and Kefalov VJ (2014) Ex vivo ERG analysis of photoreceptors using an in vivo ERG system. *Vision Res* **101**:108–117.

Watts GD, Wymer J, Kovach MJ, Mehta SG, Mumm S, Darvish D, Pestronk A, Whyte MP, and Kimonis VE (2004) Inclusion body myopathy associated with Paget disease of bone and frontotemporal dementia is caused by mutant valosin-containing protein. *Nat Genet* **36**:377–381.

Yafi FA, Sharlip ID, and Becher EF (2018) Update on the safety of phosphodiesterase type 5 inhibitors for the treatment of erectile dysfunction. *Sex Med Rev* **6**:242–252.

Yamamoto S, Tomita Y, Uruno T, Hoshida Y, Qiu Y, Iizuka N, Nakamichi I, Miyauchi A, and Aozasa K (2005) Increased expression of valosin-containing protein (p97) is correlated with disease recurrence in follicular thyroid cancer. *Ann Surg Oncol* **12**:925–934.

Yin HZ, Nalbandian A, Hsu CI, Li S, Llewellyn KJ, Mozaffar T, Kimonis VE, and Weiss JH (2012) Slow development of ALS-like spinal cord pathology in mutant valosin-containing protein gene knock-in mice. *Cell Death Dis* **3**:e374 10.1038/cddis.2012.115.

Zhang T, Mishra P, Hay BA, Chan D, and Guo M (2017) Valosin-containing protein (VCP/p97) inhibitors relieve Mitofusin-dependent mitochondrial defects due to VCP disease mutants. *eLife* **6**:e17834 10.7554/eLife.17834.

Zhang X, Feng Q, and Cote RH (2005) Efficacy and selectivity of phosphodiesterase-targeted drugs in inhibiting photoreceptor phosphodiesterase (PDE6) in retinal photoreceptors. *Invest Ophthalmol Vis Sci* **46**:3060–3066.

Zoumalan CI, Zamanian RT, Doyle RL, and Marmor MF (2009) ERG evaluation of daily, high-dose sildenafil usage. *Doc Ophthalmol* **118**:225–231.

Address correspondence to: Krzysztof Palczewski, Gavin Herbert Eye Institute, Department of Ophthalmology, Gillespie Neuroscience Research Facility, Room 2216, 837 Health Sciences Rd., Irvine, CA, 92617. E-mail: kpalczew@uci.edu; Henri Leinonen, Gavin Herbert Eye Institute, Department of Ophthalmology, Gillespie Neuroscience Research Facility, Room 2216, 837 Health Sciences Rd., Irvine, CA, 92617. E-mail: hleinone@uci.edu; or Virginia Kimonis, Department of Pediatrics, Division of Genetics and Genomic Medicine, University of California Irvine Medical Center, Hewitt Hall, Room 2038, 843 Health Sciences Rd., Irvine CA 92697. E-mail: vkimonis@uci.edu